Chapter 2
Molecular Dynamics Simulations of Nanodiamond Graphitization

Shashishekar P. Adiga, Larry A. Curtiss, and Dieter M. Gruen

Abstract Nanocarbons have attracted great interest due to their potential applications in nanoscale devices, medicine, lubrication and composite materials. Recently, nanocarbons with a variety of morphologies are reported to have been obtained after annealing nanodiamonds above 1,200 K. Here, we have investigated the transformation of 2–5 nm nanodiamond particles upon annealing using molecular dynamics simulations. The simulations show that nanodiamonds undergo annealing-induced graphitization by a progressive sp^3 to sp^2 conversion of carbon atoms that begins at the surface. The extent of this conversion depends on the size and morphology of the nanodiamond. It is found that while graphitization proceeds easily from {111} surfaces towards the core, the presence of {100} surfaces leads to residual sp^3 carbon atoms. We will also discuss different steps involved in nanodiamond graphitization, the formation of onion-like carbon and vibrational spectra of these structures.

2.1 Introduction

The science of carbon materials was immeasurably enriched some 20 years ago with the discovery of the nanocarbon family comprising fullerenes [1], nanotubes [2], ultrananocrystalline diamond [3] and more exotic forms of carbon such as nanohorns [4] and nano-onions [5]. More recently, a renewed interest in graphene has emerged. Understanding the properties of the nanocarbons including the conditions under which one form transforms into another has become an important enterprise. This is due to the existence of many basic science issues such as the close energetic relationships between all the forms of carbon as well as the tremendous potential for important applications of these materials in a wide variety of fields of application.

S.P. Adiga (✉), L.A. Curtiss, and D.M. Gruen
Materials Science Division, Argonne National Laboratory, 9700 S. Cass Avenue, Argonne, IL, 60439, USA
e-mail: shashi.adiga@gmail.com

D. Ho (ed.), *Nanodiamonds: Applications in Biology and Nanoscale Medicine*,
DOI 10.1007/978-1-4419-0531-4_2,

Among the variety of nanocarbon materials explored, nanodiamonds have spurred great excitement among researchers due to their potential applications in many engineering fields. Nanodiamonds are diamond molecules of 2–5 nm size and are found in meteorites [6] and interstellar dust [7]. Recently, nanodiamonds have been produced synthetically in the form of films [3] and powders [8–10]. Of particular success in producing large quantities of nanodiamond powder has been the detonation synthesis from explosive carbonaceous mixture. Potential applications for nanodiamonds include abrasive pastes and suspensions for high precision polishing [11], nanodiamond-polymer composites [12], wear-resistant surface coatings, cooling fluids, lubricants, and electroplating baths [13]. Another promising area for nanodiamonds is in biomedical applications [14]. A large number of potential applications, including biocompatible composites [15], drug delivery [16, 17], have been identified thanks to their superior physical and chemical properties and biocompatibility [14]. They have also been considered as potential medical agents due to high adsorption capacity, high specific surface area, and chemical inertness. They have also been explored as fluorescent biomarkers [18, 19].

Nanodiamonds are also important to the formation of nanocarbon ensembles which are being studied because of their favorable configurational entropies to improve thermoelectric performance particularly at high temperatures. Because of their high Debye temperatures, nanocarbons are among very few nanomaterials that preserve their nanocrystallinity and therefore their desirable “quantum” properties even at temperatures of 2,500 K. Despite being one of the actively researched nanomaterials, the understanding of the structure of nanodiamonds remains open. Much of the attention has been focused on the coexistence of sp^3 and sp^2 hybridized atoms, how it is affected by particle size and shape, and the ability to alter their relative amounts through the application of heat and pressure. In fact, carbon atoms in nanodiamond do not have a purely diamond structure, rather they have an intermediary structure, with a diamond-like core covered by an outer shell of graphitic/amorphous carbon [20, 21]. It has also been demonstrated that nanodiamond could transform into carbon onions [22, 23] and vice versa [24]. The structure of nanodiamond particles synthesized by detonation and their annealing induced transformation into onion-like carbons has been studied by various experimental techniques [25]. Notwithstanding many experimental studies and attempts by many theoretical efforts [26–29], the graphitization mechanism of nanodiamond is still not sufficiently understood, and so far there has been no systematic study of the graphitization of nanodiamond crystals of different shapes, sizes and hydrogen termination. There is clearly a need for a thorough study of nanodiamond graphitization and how it is likely to depend on temperature, surface termination, particle size and shape. As new applications involving surface functionalization and surface reactivity are developed, a detailed understanding of the interaction of nanodiamond/carbon-onion with its environment, as a function of the inherent changes in surface hybridization, reactivity and electrostatic potential becomes important. Particularly, in biological applications, such fundamental knowledge will help predict the potential sites for protein/DNA binding and design novel biofunctionalized nanomaterials.

In understanding the transformation between different forms of carbon at the nanoscale, it is of the essence to capture information at the atomic level. To this end, molecular modeling has played an important role in understanding the structure, stability, and phase transitions in nanocarbon materials. For example, Barnard et al. have performed extensive work on the relative stability of fullerenes, nanodiamonds and bucky diamond particles using quantum chemical calculations [30–32]. Similarly, the surface structure of nanodiamond has been studied by Hu et al. [33] using molecular dynamics (MD) simulations and Raty et al. [34, 35] using density functional theory (DFT) calculations. More recently, Barnard and Sternberg, based on the analysis of surface electrostatic potential of nanodiamond particles derived from tight-binding DFT calculations, have pointed out preferred orientations for interaction between nanodiamond particles [36].

In this chapter, we present results from classical MD simulations of graphitization of nanodiamond particles. To obtain detailed and quantitative information about the graphitization of nanodiamond, we have performed annealing simulations on several model nanodiamond structures. The emphasis is on the early stages in the heat induced sp^3–sp^2 transformation of nanodiamond particles of different size and shape. Section 2.2 contains a brief discussion of the method used including the interatomic potential. Section 2.3 describes the structure of nanodiamond particles with emphasis on surface termination and morphology. The different morphologies considered in this study are also discussed. In Sect. 2.4, results from our simulations are presented and the graphitization process is discussed with respect to the effect of temperature, shape, size and hydrogen termination. The structure of onion-like carbon (OLC) that results from graphitization and the vibrational spectra of nanodiamond particles before and after annealing is also presented.

2.2 Computational Method

The second generation reactive empirical bond order (REBO) potential [37] was used to describe the short range interaction between carbon atoms. This potential function has been widely used for hydrocarbon systems and it successfully models both sp^2 and sp^3 bonding, depending on local coordination and the degree of conjugation. Since the original REBO potential lacked both repulsive and dispersive van der Waals interactions for interatomic distances beyond which REBO is zero, later implementations included Lennard–Jones (LJ) long-range interactions. In this study, the LJ interactions were implemented with the use of cubic spline functions and parameters as described in the work by Mao et al. [38] Classical equations of motion for each atom were numerically integrated using a third-order Nordsieck predictor-corrector algorithm and a time step size 0.5 fs. The system temperature was constrained using the Langevin method [39]. The appropriateness of the interatomic potential was tested by simulating the annealing of a diamond (111) slab (a total of 21 (111) bilayers parallel to the surface) at 1,800 K. After about 600 ps

annealing at 1,800 K, the graphitization of all the layers was complete and the process resulted in a hexagonal pattern of sp^2 carbon atoms corresponding to (0001) plane of graphite with an average interlayer spacing of 3.4 Å.

2.3 Nanodiamond Structures

The nanodiamonds also referred to as ultradisperse diamonds are particles in the 2–5 nm size range. While diamond is metastable relative to graphite under atmospheric pressure, in the nanoscale regime, diamond particles less than 5 nm are more stable than graphite. For example, Barnard [30–32] compared the energies of graphite, diamond, and fullerene on the basis of density functional theory to conclude that diamond could be the stable phase of carbon clusters in the size range of 1.9–5.2 nm. Nanodiamond is often described as a crystalline diamond core with a perfect diamond lattice surrounded by an amorphous shell with a combination of sp^2/sp^3 bonds or onion-like graphite shell. Even though theoretical studies to date have considered both spherical and polyhedral nanodiamond particles, high resolution transmission electron microscope (HRTEM) images of nanodiamond have confirmed the latter [40]. Barnard et al. [30–32], using the first principles computer simulations, have shown how the polyhedral shape affects the stability of nanodiamond particles. In particular, they considered nanodiamond particles of octahedral, cuboctahedral, and cubic morphologies up to 2 nm in diameter and discussed the shape dependent stability of nanodiamond particles.

We have considered different sizes of nanodiamond particles in three shapes: octahedral (OC), truncated octahedral (TO) and cuboctahedral (CO) as shown in Fig. 2.1. The OC particle consisted of eight {111} facets (Fig. 2.1a). The TO particle consists of eight {111} facets whose two opposite vertices were truncated to produce (100) surfaces (Fig. 2.1b). The CO particle consists of eight {111} and six {100} facets (Fig. 2.1c). The models were cut from an ideal diamond crystal with the lattice constant 3.56 Å. Each of these facets in a cluster is at about the same distance from the center of the cluster.

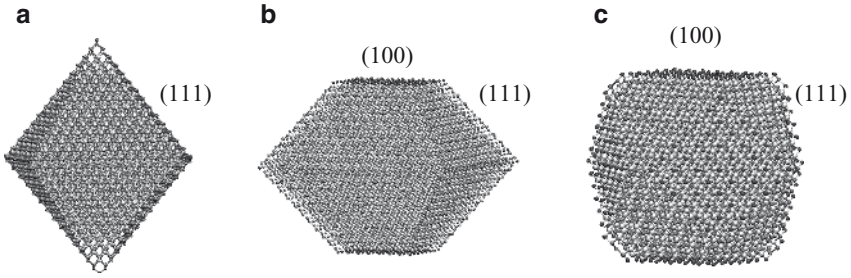

Fig. 2.1 Nanodiamond morphologies studied in this work: models of (**a**) octahedral (**b**) truncated octahedron and (**c**) cuboctahedron nanoparticles

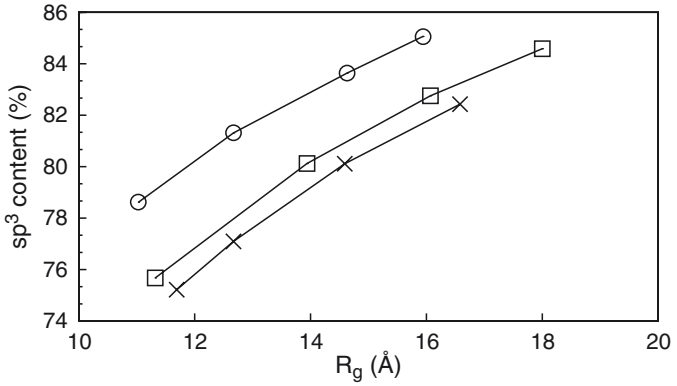

Fig. 2.2 Fraction of sp^3 hybridized atoms as a function of nanodiamond size for Octahedron (*crosses*), truncated octahedron (*squares*), and cuboctahedron (*circles*) shapes. The nanoparticles have unreconstructed surfaces. R_g is the radius of gyration of the particle

As generated, the surfaces of these nanodiamonds are unreconstructed. We first carried out MD simulations at 300 K to follow surface relaxation/reconstruction. The {111} surfaces are commonly found in the relaxed Pandey chain 2×1 reconstruction [41]. That reconstruction would yield a considerable energy gain of 0.85 eV/surface atom in the binding energy. Similarly, {100} planes usually undergo a 2×1 dimer reconstruction [42]. However, these reconstructions require substantial reorganization of the surface bonds that can only be achieved by overcoming a rather high energy barrier. Owing to this high barrier, we did not observe these reconstructions during our MD simulations at carried out at 300 K. However, as will be mentioned in the next section, we did observe these reconstructions at higher annealing temperatures before they became unstable or full of defects at temperatures above 1,800 K. After relaxation for 1 ns at 300 K, we obtained the fraction of sp^3 atoms in these nanodiamond particles. The fraction of sp^3 atoms indicates how close the nanoparticle is to the ideal diamond structure which is widely believed to determine interactions with other molecules. The variation of sp^3 content as a function of size of the nanodiamonds of OC, TO and CO morphologies is illustrated in Fig. 2.2. The size of the particle is calculated by means of radius of gyration (Rg), which is the root mean square distance of all atoms from the center of mass of the nanoparticle. It is to be noted that a higher sp^3 fraction in CO nanoparticle is due to a lower surface to volume ratio as compared to the TO and OC nanoparticles.

2.4 Results

2.4.1 Graphitization Mechanism

Our first goal is to understand the initial stages of graphitization and how the transformation proceeds in nanodiamonds. While there are several experiments reporting that nanodiamond particles can be transformed into spherical and polyhedron

carbon onions at high temperatures [22, 23, 43, 44], the mechanism of such a transformation is not well understood. In contrast, graphitization of the surface of bulk diamond has been studied extensively using both experiments and modeling. Both MD [45–47] and molecular mechanics [48] simulations of graphitization of the diamond (111) surface have suggested that the formation of fullerene-like or graphitic surface structure is one of the most effective ways of minimizing the surface free energy at high temperatures. In addition to being a dominant face in the morphology of diamond, the reason for {111} planes playing a prominent role in the graphitization process stems from the fact that there is a close geometrical relationship between them and the individual graphene sheets. The diamond (111) plane contains a pair of atomic layers and resembles "puckered" graphite (0001) layer with a hexagonal pattern. This geometrical relationship together with the lengthening of carbon–carbon bonds from 1.42 Å in graphite to 1.54 Å in diamond results in the near epitaxial relations.

Vita et al. using ab initio molecular dynamics (MD) methods, showed that at flat diamond (111) surfaces graphitic features can be formed at 2,500 K by a direct transformation [45]. They showed that the decisive step in initiating the transformation is the breaking of some of the bonds between the first and second bilayers at the surface. To explain why a (111) surface readily undergoes graphitization, Kuznetsov et al. [48] compared graphitization on diamond (111) and (110) surfaces using the cluster models. Their calculations showed that graphitization of (111) surface is more favorable by 0.24 eV/surface atom than graphitization of a (110) surface. Also, the barrier for transformation was found to be higher for the (110) surface by 0.93 eV/surface atom. These calculations demonstrated that graphitization of a (111) surface is clearly preferred over that of a (110) surface. In addition to the direct transformation, they have also suggested a "zipper-like" migration mechanism in which two graphene sheets are formed from three diamond (111) planes with the carbon atoms of the middle diamond layer being distributed equally between the two growing graphitic sheets as the graphite diamond interface advances. However, the relative importance of these to mechanisms or any other mechanism in nanodiamond graphitizaton is yet to be determined.

Recently, there have been a few modeling studies concerning the heat induced graphitization of nanodiamond particles. Fugaciu et al. investigated graphitization of nanodiamonds with a diameter in the 1.2–1.4 nm range using the tight-binding DFT [26]. Lee et al. [27] employed tight-binding MD simulations and found that nanodiamonds of ~1.4 nm diameter transformed into a tube-shaped fullerene via annealing. These simulations provided important information on the nature of transformation of nanodiamond particles which consist of several hundred carbon atoms. Modeling graphitization of experimentally relevant nanodiamonds, i.e., in the size range 3–5 nm, is currently beyond the reach of ab initio methods. On the other hand, Bro'dka et al. investigated the graphitization of a 3 nm spherical nanodiamond annealed at temperatures 1,200, 1,500 and 1,800 K [28]. However, it was later demonstrated by Leyssale and Vignoles [29] that the Berendsen thermostat used by these authors is not suitable to the study of isolated nanoparticles and suggested using a more suitable thermostat. These studies also did not incorporate repulsive and dispersive van der Waals interactions,

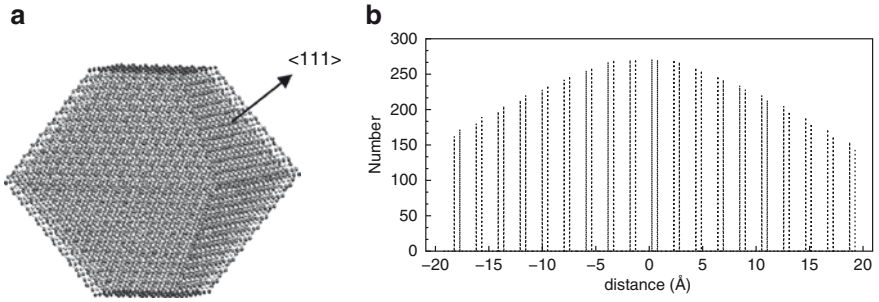

Fig. 2.3 Structure of a TO nanodiamond consisting of 8,459 atoms prior to annealing: (**a**) atomic model with <111> direction marked and (**b**) number of atoms as a function of distance from the origin along <111> direction, the diamond (111) double layers are clearly seen

which are thought to be important in modeling the graphitic phase. We have addressed the shortcomings of the previous classical MD studies by using both a more suitable Langevin thermostat and a more appropriate interatomic potential that includes LJ non-bonded interactions as described in Sect. 2.2.

Before we discuss the dependence of the extent of graphitization on temperature, particle size and shape, and hydrogen termination, we will demonstrate the progressive transformation of predominantly sp^3 atoms into sp^2 atoms with the example of a TO nanodiamond particle (8,459 atoms) annealed at 1,800 K. The initial structure of the nanodiamond particle is shown in Fig. 2.3a. Also, the ideal diamond structure of the nanodiamond particle is further characterized by plotting the number of atoms as a function of distance from the origin along the <111> direction (Fig. 2.3b). The plot shows the characteristic double peaks corresponding to diamond (111) bilayers and that the distance between two adjacent bilayers is 2.02 Å (interplanar distance).

In Fig. 2.4, the time evolution of graphitization is illustrated with a series of snapshots of the nanodiamond particle after $t=0$, 5, 10, 20, 200, and 800 ps of annealing at $T=1{,}800$ K. The 2-, 3-, and 4-coordinated carbon atoms are colored black, gray and silver, respectively. The two (100) surfaces undergo 2×1 reconstruction within the first 5 ps of annealing. Graphitization begins at {111} facets on the surface and progresses towards the center of the nanodiamond particle. Figure 2.5 further illustrates the initial stages of the graphitization process that involves progressive disappearance of the layered structure characteristic of diamond lattice. The plots represent number of atoms as a function of distance from the center of mass (COM) of the particle along the <111> direction. The plots are given for annealing times $t=10$, 200, and 400 ps at $T=1{,}200$, 1,500, and 1,800 K. The graphitization process is initiated at the surface (111) layer with thermal displacements of surface atoms from their equilibrium positions. During the initial period of about 10 ps, the diamond particle graphitizes at the surface forming graphitic layers enclosing a diamond core. Then, the diamond short-range order in the core of the particle gets more and more disordered as indicated by straightening of

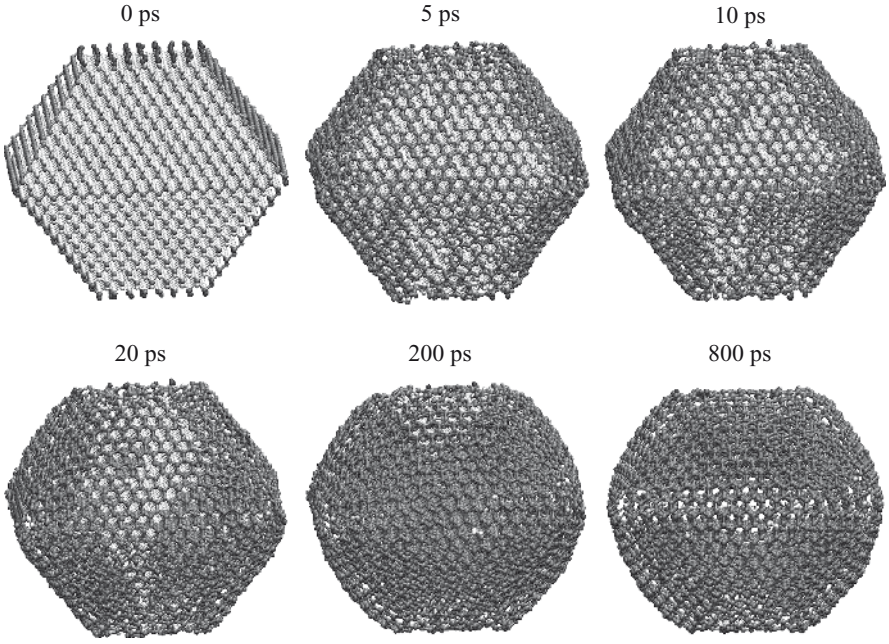

Fig. 2.4 Initial stages of graphitization. Snapshots from MD simulations of a truncated octahedral cluster (8,459 atoms) after $t = 0$, 5, 10, 20, 200, and 800 ps of annealing at 1,800 K. The 2-, 3-, and 4-coordinated carbon atoms are colored black, gray and silver, respectively. The TO nanoparticle relaxed at 300 K for 1 ns was used as the starting structure ($t = 0$ ps). The two (100) surfaces (*top* and *bottom*) undergo 2×1 reconstruction within the first 5 ps of annealing. Graphitization begins at {111} facets on the surface and progresses towards the center of the nanodiamond particle. The regions underneath surface (100) facets (top and bottom) undergo a slower transformation and contain residual sp^3 atoms. The (111) facets become curved as a result of annealing

the puckered (111) bilayers into a single layer and broadening of the peaks. Once a graphitic region is formed within the surface layer, the graphitization starts to proceed towards the center in a direction perpendicular to the (111) surface layer. A similar mechanism for the progress of graphitization has previously been observed in MD simulations of planar diamond (111) surfaces [45].

A key feature of the graphitization process is the formation of graphitic ‘‘blister’’ on the surface. As the outermost layer is delaminated it bulges out and assumes a convex shape that is under tensile stress. This is evident from the larger interplanar distance between the top two layers as illustrated in the density profiles (Fig. 2.5). Evidence for the formation of such curved graphitic features has been provided by HRTEM images of annealed nanodiamond particles [25].

Further information on the evolution of the graphitization during the early stage of annealing is analyzed in terms of the fraction of carbon atoms with trivalent coordination (sp^2) as a function of time at annealing temperatures $T = 1{,}200$, 1,500,

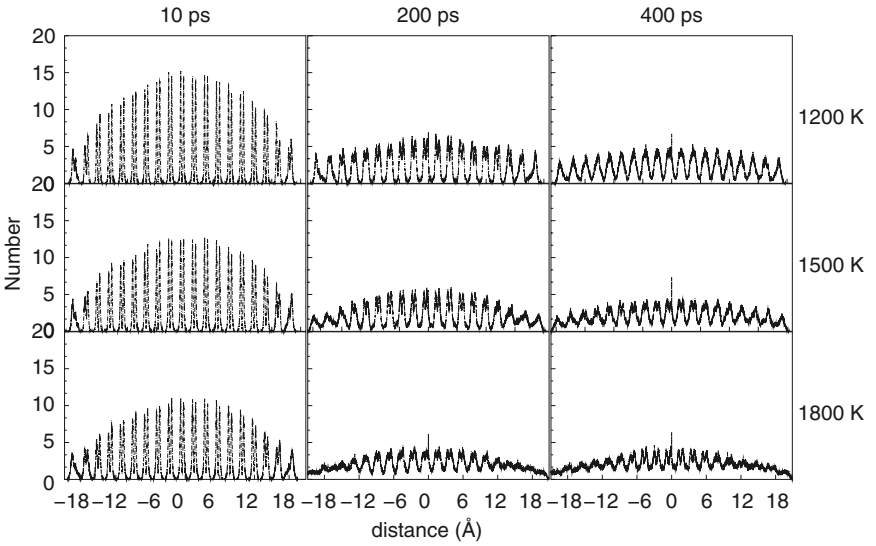

Fig. 2.5 The evolution of graphitization at different temperatures. The number of atoms along <111> as a function of distance from the center of mass of the particle is plotted at 10 (*left*), 200 (*center*) and 400 (*right*) ps after annealing at 1,200 (*top*), 1,500 (*middle*) and 1,800 (*bottom*) K

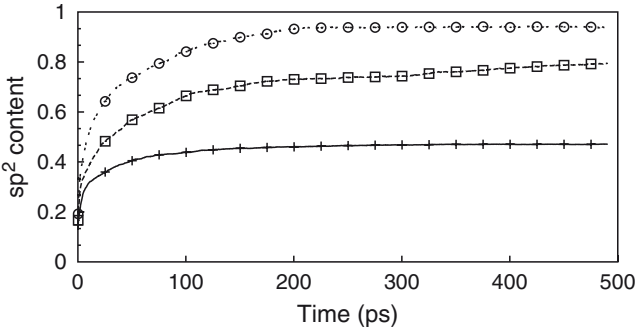

Fig. 2.6 Progression of sp^3–sp^2 conversion during the initial stages of annealing. The fraction of three coordinated carbon atoms in the TO nanodiamond particle (8,459 atoms) is plotted as function of annealing time at $T = 1{,}200$ (*crosses*), 1,500 (*squares*), and 1,800 (*circles*) K

and 1,800 K (Fig. 2.6). Two carbon atoms are considered bonded if the distance between them is less than 1.85 Å, corresponding to the first minimum in the radial distribution function of graphite. At 1,200 K, about 47% of all atoms have trivalent coordination. Increasing the temperature to 1,500 K accelerated the sp^3 to sp^2 conversion, and eventually about 80% of carbon atoms had trivalent coordination. The increase of the annealing temperature to 1,800 K increased the fraction of three coordinated atoms to 95%. For all temperatures studied, the fraction of sp^2 atoms did not change beyond about 500 ps.

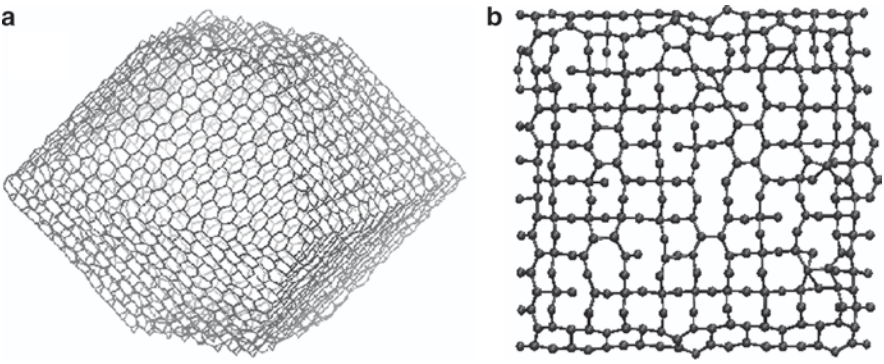

Fig. 2.7 The final structure of the TO nanodiamond cluster after 2 ns of annealing at 1,800 K. The cluster is predominantly sp^2 (95%). (**a**) A wire frame representation showing graphitic hexagonal pattern formed on the original nanodiamond (111) facets. (**b**) Surface layer corresponding to the (100) facet of the original nanodiamond

The final structure after 2 ns of annealing at 1,800 K shown in Fig. 2.7a retained the original TO shape to a large extent. It consisted of nested cages of mostly three coordinated atoms characterized by graphene-like hexagonal network structure parallel to the original nanodiamond {111} facets. Parallel to the two {100} facets of the nanodiamond, the resulting layers contained carbon atoms with mixed coordination. The surface layer corresponding to the (100) facet of the original nanodiamond is shown in Fig. 2.7b. It has a mix of 3, 5, 6, 7 and 8 sided polygons.

2.4.2 Factors Affecting Graphitization

2.4.2.1 Annealing Temperature

Many experimental studies have suggested that nanodiamond particles transform into graphitic structures after annealing at temperatures ranging from 1,373 to 2,173 K [49, 50]. The extent of graphitization, however, depended on the temperature. For example, it has been reported that annealing at 1,373 K results in partial graphitization and complete transformation happens only for temperatures above 1,673 K [50]. Incomplete graphitization has been indicated by sp^3 signal from electron energy loss spectroscopy, X-ray diffraction or Raman spectroscopy. The residual sp^3 signal has been variously attributed to the presence of dangling bonds, or atoms connecting small sp^2 domains, or the presence of a diamond core surrounded by graphitic shells [20, 21]. To explore the effect of temperature on the extent of transformation, the cuboctahedron nanoparticle with 3,130 atoms and the octahedron nanoparticle with 4,495 atoms were annealed at temperatures $T = 1{,}200$, 1,500, 1,800 and 2,500 K. In Fig. 2.8, a plot of the fraction of sp^2 atoms vs annealing temperature for an annealing time of 2 ns is given. For the octahedron, the fraction

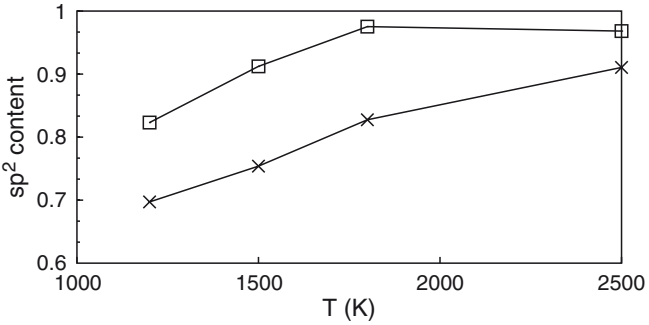

Fig. 2.8 The effect of annealing temperature on the extent of graphitization. The fraction of sp^2 atoms in a CO with 3,130 atoms (*crosses*) and an OC with 4,495 atoms (*squares*) nanodiamonds as a function of annealing temperature is plotted. The annealing was performed for 2 ns

of 3-coordinated sp^2 carbon atoms increased from 0.82 at 1,200 K to 0.97 at 1,800 K and slowly plateaued off. The CO particle, on the other hand, increased its sp^2 fraction from 0.69 at 1,200 K to 0.91 at 2,500 K. As discussed in the next paragraph, the residual sp^3 atoms belong mainly to the untransformed regions below {100} facets of the CO nanoparticle and hence, particle shape plays a big role in the extent of transformation, besides temperature. Whereas in the OC particle, the small amount of sp^3 atoms are mostly isolated and often connect two adjacent graphitic shells.

In contrast to our simulation results, experimental studies have reported a complete transformation to spherical onion-like carbons at 2,000 K. For example, a nanodiamond particle of diameter ~5 nm was transformed into spherical carbon onions at 2,000 K and into polyhedron carbon onions at 2,300 K [44]. The final structures obtained from our 2 ns long simulations contain residual sp^3 atoms. However, it is possible that, if the simulations can be performed for a sufficiently long time to allow for large scale rearrangement of atoms between the graphene layers, a spherical carbon onion shall be obtained. It is also possible that the presence of defects and surfaces and contact with other nanodiamond particles may facilitate the complete transformation observed in the experiments.

2.4.2.2 Nanodiamond Shape

As previously mentioned, the transformation of {111} planes occurs more easily as compared to {110} or {100} planes. The fact that transformation rate of the {111} diamond planes to graphite-like sheets is higher than those of the other planes, which has been confirmed by both experimental and theoretical investigations. For example, Pantea et al. [51] while studying the graphitization of single crystal diamond at different pressures and temperatures, observed oriented growth of graphite on {111} faces when compared with the disoriented graphitic layers on {100} faces, and suggested dissimilar graphitization mechanisms for different diamond faces.

Since the surface of nanodiamond particles, depending on the morphology, can be terminated with different facets, it is important to explore how graphitization is affected by their shape. To investigate this, we considered OC, CO and TO nanodiamond particles of the same size in terms of the surface to nanodiamond center of mass (COM) distance. These particles with 4,495, 3,864, and 3,130 atoms, respectively, were annealed at 1,800 K.

Because of the difference in the barrier and the energy of transformation between different facets, it is interesting to probe how morphology plays a role in the extent of graphitization. In Fig. 2.9, we illustrate this with OC, TO and CO nanoparticles of roughly the same size (i. e. distance from the center of mass at which the nanoparticle facets lie is ~15 Å). These particles consisted of 4,495, 3,864, and 3,130 atoms, respectively. In the bottom panel of Fig. 2.9, a plot of the fraction of sp^2 atoms as a function of annealing time is given for these three nanoparticles. The OC, TO and CO nanoparticles rapidly reach sp^2 fractions of 0.97, 0.95, and 0.84, respectively, within 100 ps. In addition to the extent of transformation, it is apparent

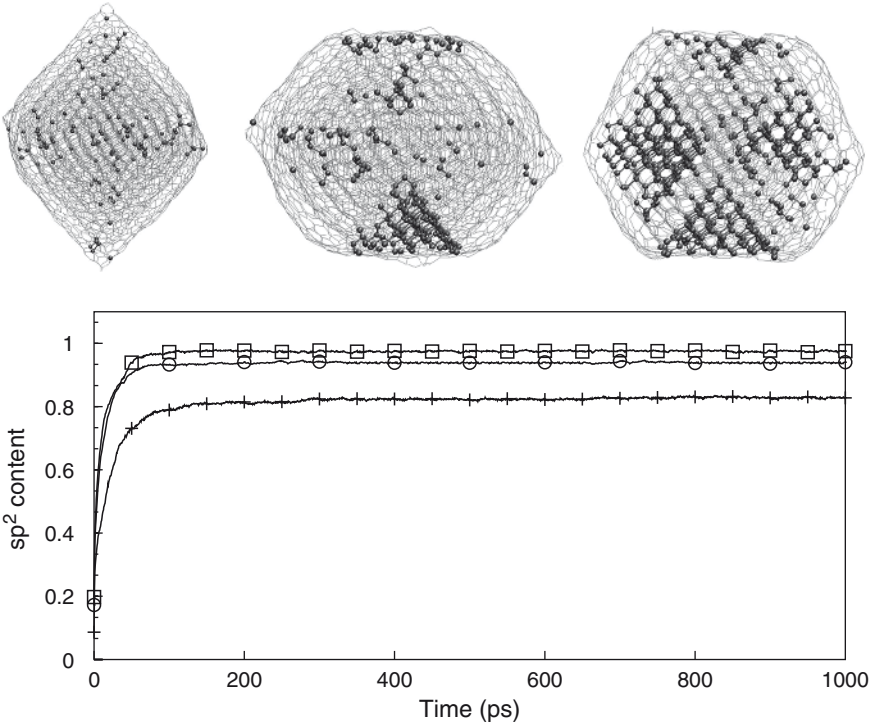

Fig. 2.9 The effect of particle shape on nanodiamond graphitization. *Top*: Snapshots of the nanoparticles octahedron (OC) with 4,495 atoms (*left*), truncated octahedron (TO) with 3,864 atoms (*center*), and cuboctahedron (CO) with 3,130 atoms (*right*) after 2 ns of annealing at 1,800 K. The 4-coordinated atoms are represented by ball-stick model to illustrate the presence of residual diamond-like regions mostly beneath {100} surfaces. Bottom: The evolution of sp^2 fraction for OC (*squares*), TO (*circles*) and CO (*crosses*) nanoparticles with annealing time

that the rate of transformation in the initial 100 ps is much higher for OC which has 100% {111} termination. The TO and CO nanoparticles with larger {100} surface coverage graphitize to a smaller extent is further illustrated with MD snapshots in the top panel of Fig. 2.9. These snapshots of the three nanoparticles are taken after 2 ns annealing at 1,800 K. The 3- and lower coordinated atoms are shown in with wireframe representation, whereas the 4-coordinated atoms are represented by ball-stick model to illustrate the location of residual sp^3 atoms. In the case of OC, the residual sp^3 atoms are sparse and isolated and they connect two neighboring graphitic shells. In contrast, the residual sp^3 atoms in TO and CO nanoparticles are often part of larger diamond domains and they represent untransformed regions below {100} surfaces. In the case of CO, for example, six such sp^3 regions are present (two on the back side), that lie underneath the six {100} surfaces of the original nanodiamond particle. Hence, the presence of {100} facets along with {111} facets has the effect of arresting the otherwise fast transformation of nanodiamond particles leading to the residual diamond like regions.

2.4.2.3 Nanodiamond Size

Graphitization of diamond also strongly depends on the diamond particle size. Crystals with smaller sizes graphitize faster [52]. In annealing the experiments conducted by Xu et al., nanodiamonds were annealed in different gas atmospheres [53]. They found that the graphitization of nanodiamond in argon begins at 940 K, which is significantly lower than the value 1,800 K for bulk diamond. The difference was attributed to the large surface-to-volume ratio and high thermal conductivity of nanodiamond. In Fig. 2.10, the evolution of graphitization is analyzed for CO nanoparticles consisting of 2,067 (CO1), 3,130 (CO2) and 6,232 (CO3) atoms at 1,800 K. The values obtained for the fraction of sp^2 atoms for the three

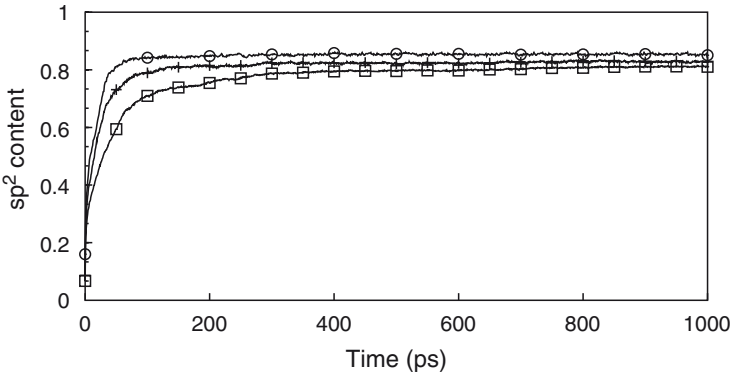

Fig. 2.10 Effect of nanoparticle size. The fraction of sp^2 atoms is plotted as a function of annealing time for cuboctahedron nanoparticles consisting of 2,067 (*circles*), 3,130 (*crosses*) and 6,232 (*squares*) atoms at $T = 1{,}800$ K

nanoparticles are 0.86, 0.84 and 0.83 for CO1, CO2, and CO3, respectively. Given the relatively smaller size range we have considered, the small change in the extent of graphitization for the three sizes is reasonable.

2.4.2.4 Hydrogen Termination

The discussion so far considered graphitization of bare nanodiamond particles. Hydrogen termination is expected to stabilize the nanodiamond structure. For example, Russo et al. [54] performed DFT calculations of hydrogenated nanodiamonds of both the octahedral and cuboctahedral morphologies and found that in addition to passivating the surface hydrogenation stabilizes diamond structure against graphitization. To probe this, we considered a TO nanoparticle with 8,459 carbon atoms terminated with 1,454 hydrogen atoms. The annealing was performed at 1,800 K for 2 ns. The resulting atom density profile along the <111> direction is shown in Fig. 2.11. The {111} bilayers of the nanodiamond particle remain intact as opposed to the unpassivated nanodiamond particle (Fig. 2.5).

2.4.3 Onion-Like Carbons

Carbon onions are multilayered spherical nanostructures made up of nested fullerene cages. A variety of methods have been used to make carbon onions including, for example, high-energy electron irradiation, arc discharge and thermal treatment of carbonaceous materials. This class of nanocarbons has been referred to with multiple

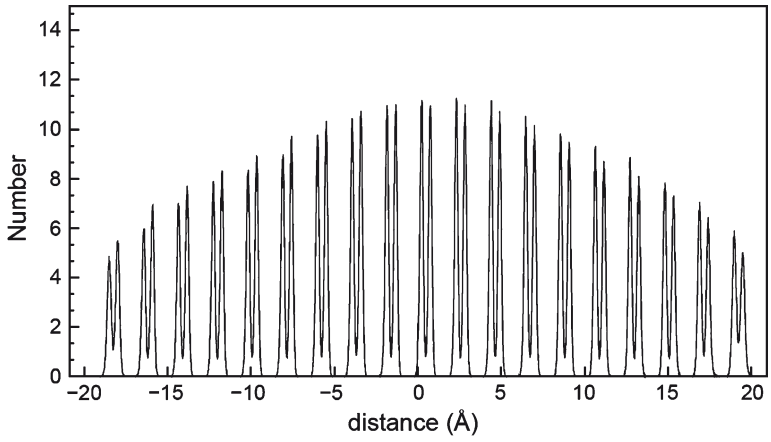

Fig. 2.11 Effect of hydrogen termination. The number of atoms along <111> as a function of distance from the center of mass of the particle is plotted for the hydrogen terminated TO particle with 8,459 carbon atoms annealed at 1,800 K for 2 ns

names including carbon onions, carbon nano-onions (CNO), multilayer fullerenes, onion-like fullerenes and onion-like carbon (OLC). Recently, the transformation of detonation nanodiamond (DND) particles into the nested fullerene-like carbon structures at temperatures above 800 K has been explored as a way to make the nanographitic structures. In the literature, these multilayered cages obtained by annealing of DNDs has been referred to as OLC, mainly to distinguish them from the ideal carbon onions consisting of layers of enclosed fullerene molecules of different sizes [22]. The predominantly sp^2 hybridized structures obtained in our simulations as a result of annealing nanodiamonds closely represent the OLC structures described in the literature. In this context, we will discuss the structure obtained after annealing the OC1 cluster at 1,800 K for 2 ns.

The final structure shown in Fig. 2.12, consists of seven concentric graphitic shells around a few central atoms which can be better described as a small carbon cluster. The structure has ~3% residual sp^3 atoms, a majority of which link two adjacent graphitic shells. The OLC structure more or less retains the original octahedral shape of the nanodiamond. In Fig. 2.12, the average distance $D_{i,\,i+1}$, between layers i and i+1, is plotted as a function of layer index i. The layers are numbered from the center. The interlayer distance between the two outermost layers is about 2.9 Å, close to the equilibrium distance between two graphene sheets, whereas the inter layer distance towards the center is ~2.35 Å , slightly more than that for diamond (111) planes (=2.06 Å). Based on the interlayer distances, one can expect a relatively high pressure region at the center of the onion. It is interesting to point out that Banhart and Ajayan [55] demonstrated the reverse transformation of the cores of carbon onions to diamond via electron irradiation at temperatures above 900 K. Unlike the nanodiamond-OLC conversion that starts at the surface of the nanoparticle, the nucleation of sp^3 diamond region occurs at, the center of the carbon onion. Banhart [56] proposed that the high pressure in the concentric-shell fullerene is a prerequisite for the nucleation of diamond. Additionally, he also speculated about the presence of sp^3 cross links between the adjacent graphitic shells.

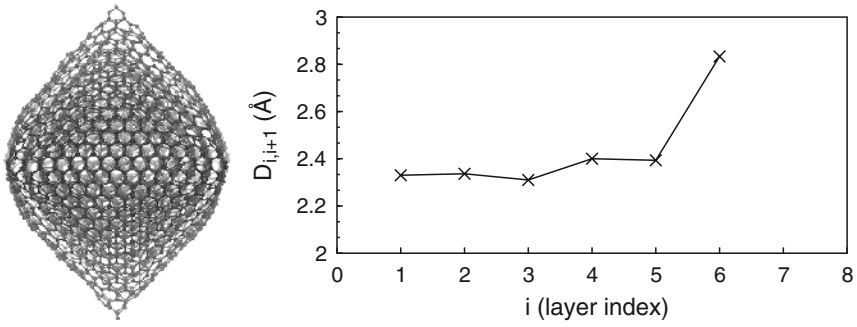

Fig. 2.12 The structure of onio-like carbon obtained after annealing an OC nanodiamond particle. *Left*: A ball-stick representation of the cluster shows nested graphitic cages. *Right*: Plot of interlayer distance as a function of layer index

Perhaps it is worthwhile to point out a key aspect of nanodiamond to OLC transformation to better understand why the interlayer distance in the multishell graphitic structure resulting from nanodiamond annealing is less than 3.37 Å. Diamond to graphite transformation is characterized by a substantial increase in volume, as diamond is ~1.53 times denser than graphite. Let us consider the transformation of an octahedral nanodiamond particle with all {111} termination such as the one discussed in this section. Such a nanodiamond cluster will essentially consist of nested cages made up of diamond (111) bilayers. The first step in graphitization of these individual cages involves straightening of the buckled (111) layer that results in merging of the bilayers into a single layer, structurally similar to a polyhedral graphene cage. The next step involves an increase in the distance between the two consecutive shells from 2.06 Å, corresponding to the diamond (111) interplanar distance, to 3.37 Å of the distance between (0001) planes in graphite. This will require a substantial volume expansion that leads to a decrease in the number of atoms per unit area in the expanding layer. The deficit in atom density created because of the expansion has to be compensated for in order to relieve the surface tension. These "extra" atoms needed in the outer layers can be hypothesized to be supplied through a flow of atoms from the inner layers to the outer. We can intuitively see how such a process can lead to OLCs with hollow cores. However, it can also be speculated that such a process has a large energy barrier due to substantial rearrangement of atoms. Perhaps, the presence of the other particles/ surface in the vicinity can relieve the surface tension of the graphitizing nanodiamond particle and assist in the completion of the transformation.

Another feature we have not considered in this study is the presence of defects. It has been reported that graphitization can be initiated at surface defects. For example, stepped {111} surfaces are graphitized spontaneously [57]. Based on the MD simulations of bulk diamond surfaces it has been proposed that twin boundaries also can promote spontaneous graphitization [47]. In future studies, it will be interesting to study the effect of defects on the graphitization of nanodiamond particles.

Further information on the structure of onion-like carbon can be obtained by analyzing the radial distribution function, which gives the average number of atoms as a function of distance around any given atom. The radial distribution function $g(r)$ is defined as $g(r) = \frac{\langle n(r, \Delta r) \rangle}{4\pi r^2 \Delta r \rho}$ where $n(r, \Delta r)$is the average number of atoms in a spherical shell of thickness Δr at a distance r from an atom and is an average over all atoms sampled over 100 ps. The number density of atoms ρ is taken as the value corresponding to the mass density of diamond (3.53 g/cm^3). A value of $\Delta r = 0.01$ Å is used. Figure 2.13 shows the radial distribution functions ($g(r)$) for the octahedral nanodiamond before (*solid line*) and after (*dotted line*) annealing at 1,800 K respectively. The $g(r)$ analysis was obtained for both structures from simulations performed at 300 K. The first four peaks in $g(r)$ for the cluster annealed at 1,800 K are at 1.41, 2.45, 2.85 and 3.76 Å. These peak positions correspond well with the first to fourth neighbor distances in a graphene sheet and may be seen as

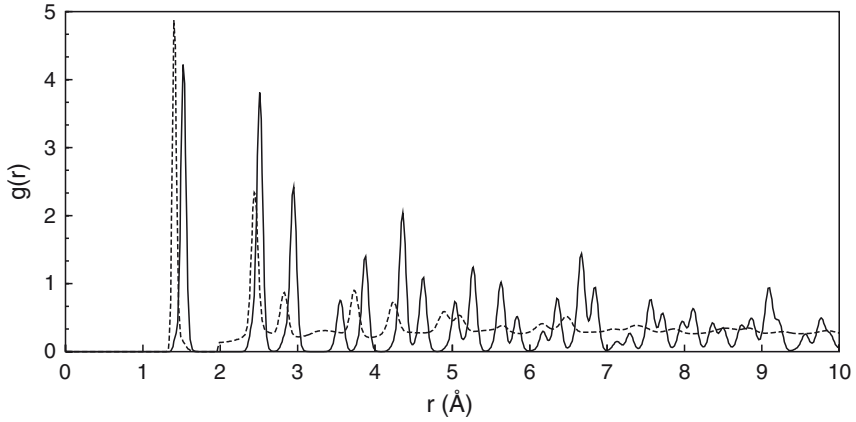

Fig. 2.13 The radial distribution function for 4,495 atom octahedral nanodiamond cluster at $T = 300$ K before (*solid line*) and after (*dotted line*) annealing at 1,800 K

an indication that a phase transition to sp^2 carbon has occurred. It is important to note that, unlike periodic structures, the nanoparticle $g(r)$ calculated here does not assume a value of 1.0 at long distances.

2.4.4 Vibrational Spectra

Raman spectroscopy has been a key technique used for studying the nature of the c–c bond as it is able to distinguish between the sp^2 and sp^3 content quite effectively. To illustrate how annealing induced graphitization changes the vibrational properties of nanodiamond particles, we have calculated the vibrational power spectra (vibrational densities of states) by following the atomic trajectories during the MD simulation. The vibrational density of states (VDOS) was determined by calculating the Fourier transform of the velocity auto correlation function (VACF). The VACF gives the correlation between the velocity of an atom at time $t = 0$ and the velocity of an atom at time $t = t$. It is important to point out that the computed VDOS and the experimental Raman vibrational spectra are not identical, as the former contains all vibrational atomic motions, and the latter have only Raman active modes with intensities that are different than the computed VDOS. However, the calculated band positions and experimental spectra can be compared. To calculate VACF, the velocities were sampled every time step for 10 ps.

In Fig. 2.14, VDOS at 300 K for the CO nanoparticle with 3,130 atoms before and after annealing at 1,800 K are compared. The VDOS for the nanodiamond particle is characterized by a strong peak at 1,380 cm^{-1}, corresponding to sp^3 bond stretching. The experimental number for this peak is lower, in the range 1,320–1,335 cm^{-1}. Another noteworthy feature is at around 1,620 cm^{-1}, which can be attributed to the

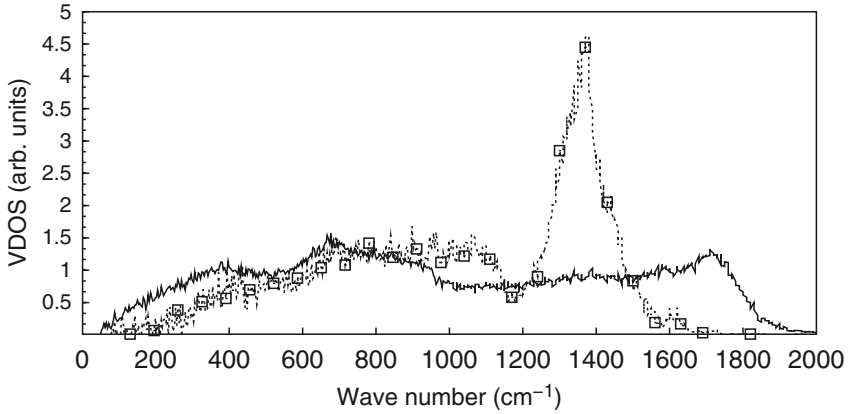

Fig. 2.14 Vibrational density of states obtained for the cuboctahedral nanodiamond cluster with 3,130 atoms: before (*dotted line* with *squares*) and after (*solid line*) annealing at 1,800 K

undercoordinated surface atoms. The key difference in the VDOS of the annealed structure is the diminishing and the broadening of the diamond peak (1,380 cm^{-1}) and appearance of a broad peak at 1,730 cm^{-1}. This peak from sp^2 carbon atoms reflects the effect of annealing. This signature for sp^3–sp^2 transformation provided by the VDOS of the nanodiamond particle is comparable with the previous experimental Raman studies used to monitor the nanodiamond graphitization [25].

2.5 Summary and Outlook

In summary, the classical MD simulations study discussed above provides insights into the structure of nanodiamonds and their annealing induced transformation into graphitic carbon. The simulations show, as has been indicated by previous experiments, that graphitization begins at nanodiamond surface and progresses to the center. The graphitization process preferentially advances perpendicular to {111} surfaces over {100} surfaces. In addition to {100} surfaces, hydrogen termination is found to stabilize sp^3 hybridization at high temperatures. The results show a strong correlation between shape, annealing temperature, surface hydrogenation and the extent of graphitization.

From the biomedical applications perspective, it is desirable to investigate the nature of bonding at the surface of nanodiamonds and their interaction with biomolecules and eventually design tailor made interfaces between them. In this respect, as a logical extension of this work, it is important to explore the interaction of proteins and nucleic acids with nanodiamond particles and investigate the effect of their relative sp^2/sp^3 content. MD simulations can provide valuable information on the nature of interaction between nanocarbon and how nanodiamond particles influence the

structure and function of biomolecules. The future holds great promise for the development of multiscale methods that allow modeling an ensemble of large biomolecules interacting with nanocarbon particles and make the goal of complete understanding of the nature of nanodiamond-biomolecule interfaces feasible.

Acknowledgments This work was supported by the US Department of Energy's Office of Basic Energy Sciences, under contract no. DE-AC02-06CH11357. Use of computer resources from Argonne National Laboratory Computer Resource Center and US DOE National Energy Research Supercomputer Center is gratefully acknowledged.

References

1. Kroto HW, Heath JR, O'brien SC, Curl RF, Smalley RE (1985) Nature 318:162–163
2. Iijima S (1991) Nature 354:56–58
3. Gruen DM, Liu S, Krauss AR, Luo J, Pan X (1994) Appl Phys Lett 64:1502–1504
4. Iijima S, Yudasaka M, Yamada R, Bandow S, Suenaga K, Kokai F, Takahashi K (1999) Chem Phys Lett 309:165–170
5. Ugarte D (1992) Nature 359:707–709
6. Lewis RS, Tang M, Wacker JF, Anders E, Steel E (1987) Nature 326:160–162
7. Dai ZR, Bradley JP, Joswiak DJ, Brownlee DE, Hill HGM, Genge MJ (2002) Nature 418:157–159
8. Greiner NR, Philips DS, Johnson JD, Volk F (1988) Nature 333:440–442
9. Vereschagin AL, Sakovich GV, Komarov VF, Petrov EA (1993) Diam Relat Mater 3:160–162
10. Kuznetsov VL, Chuvilin AL, Moroz EM, Kolomiichuk VN, Shaikhutdinov ShK, Butenko YuV (1994) Carbon 32:873–882
11. Artemov AS (2004) Phys Solid State 46:687–695
12. Shenderova O, Tyler T, Cunningham G, Ray M, Walsh J, Casulli M, Hens S, McGuire G, Kuznetsov V, Lipa S (2007) Diam Relat Mater 16:1213–1217
13. Dolmatov VY (2001) Russ Chem Rev 70:607–626
14. Schrand AM, Huang H, Carlson C, Schlager JJ, Sawa EO, Hussain SM, Dai L (2007) J Phys Chem B 111:2–7
15. Khabashesku VN, Margrave JL, Barrera EV (2005) Diam Relat Mater 14:859–866
16. Kam NWS, Jessop TC, Wender PA, Dai HJ (2004) J Am Chem Soc 126:6850–6851
17. Huang H, Pierstorff E, Osawa E, Ho D (2007) Nano Lett 7:3305–3314
18. Narayan RJ, Wei W, Jin C, Andara M, Agarwal A, Gerhardt RA, Shih CC, Shih CM, Lin SJ, Su YY, Ramamurti Y, Singh RN (2006) Diam Relat Mater 15:1935–1940
19. Yu SJ, Kang MW, Chang HC, Chen KM, Yu YC (2005) J Am Chem Soc 127:17604–17605
20. Kuznetsov VL, Chuvilina AL, Butenkoa YV, Stankusb SV, Khairulinb RA, Gutakovskiic AK (1998) Chem Phys Lett 289:353–360
21. Tomita S, Burian A, Dore JC, LeBolloch D, Fujii M, Hayashi S (2002) Carbon 40:1469–1474
22. Kuznetsov VL, Chuvilin AL, Butenko YV, Malkov IY, Titov VM (1994) Chem Phys Lett 222:343–348
23. Aleksenskii AE, Baidakova MV, Vul' A Ya, Siklitskii VI (1999) Phys Solid State 41:668–671
24. Banhart F, Fuller T, Redlich Ph, Ajayan PM (1997) Chem Phys Lett 269:349–355
25. Mykhaylyk OO, Solonin YM, Batchelder DN, Brydson R (2005) J Appl Phys 97:074302
26. Fugaciu F, Herman H, Deifert G (1999) Phys Rev B 60:10711–10714
27. Lee GD, Wang CZ, Yu J, Yoon E, Ho KM (2003) Phys Rev Lett 91(26):265–701
28. Bro'Dka A, Zerda TW, Burian A (2006) Diam Relat Mater 15:1818–1821
29. Leyssale J-M, Vignoles GL (2008) Chem Phys Lett 454:299–304
30. Barnard AS, Russo SP, Snook IK (2003) Diam Relat Mater 12:1867–1872

31. Barnard AS, Russo SP, Snook IK (2003) Phys Rev B 68:073406
32. Barnard AS (2006) Stability of Nanodiamond In: Shenderova OA, Gruen DM (eds),Ultrananocrystalline diamond: synthesis, properties and applications. William Andrew Publishing, New York, pp 117–154
33. Hu Y, Shenderova OA, Hu Z, Padgett CW, Brenner DW (2006) Rep Prog Phys 6:1847–1895
34. Raty JY, Galli G (2003) Nat Mater 2:792–795
35. Raty JY, Galli G, Bostedt C, van Buuren TW, Terminello LJ (2003) Phys Rev Lett 90:037401
36. Barnard AS, Sternberg M (2007) J Mater Chem 17:4811–4819
37. Brenner DW, Shenderova OA, Harrison JA, Stuart SJ, Ni B, Sinnott SB (2002) J Phys: Condens Matter 14:783–802
38. Mao Z, Garg A, Sinnott SB (1999) Nanotechnology 3:273–277
39. Adelman SA, Doll JD (1976) J Chem Phys 64:2375–2388
40. Tyler T, Zhirnov VV, Kvit AV, Kang D, Hren JJ (2003) Appl Phys Lett 82:2904–2906
41. Pandey KC (1982) Phys Rev B 25:4338–4341
42. Zapol P, Curtiss LA, Tamura H, Gordon MS (2004) Theoretical studies of growth reactions on diamond surfaces In: Curtiss LA, Gordon MS (eds) Computational materials chemistry: methods and applications. Kluwer Academic Publishers, London, pp 266–307
43. Tomita S, Fuji M, Hayashi S (2002) Phys Rev B 66:245–424
44. Tomita SS, Fuji M, Hayashi S, Yamamoto K (1999) Chem Phys Lett 305:225–229
45. Vita AD, Galli G, Canning A, Car R (1996) Nature 379:523–526
46. Wang CZ, Ho KM, Shirk MD, Molian PA (2000) Phys Rev Lett 85:4092–4095
47. Jungnickel G, Porezag D, Frauenheim Th, Heggie MI, Lambrecht WRL, Segall B, Angus JC (1996) Phys Status Solidi A 154:109–125
48. Kuznetsov VL, Zilberberg IL, Butenko YuV, Chuvilin AL, Segall B (1999) J Appl Phys 86:863–870
49. Qian J, Pantea C, Huang J, Zerda TW, Zhao Y (2004) Carbon 42:2691–2697
50. Qiao Z, Li J, Zhao N, Shi C, Nash P (2006) Scr Mater 54:225–229
51. Pantea C, Qian J, Voronin GA, Zerda TW (2002) J Appl Phys 91:1957–1962
52. Chen PW, Ding YS, Chen Q, Huang FL, Yun SR (2000) Diam Relat Mater 9:1722–1725
53. Xu NS, Chen J, Deng SZ (2002) Diam Relat Mater 11:249–256
54. Russo SP, Barnard AS, Snook IK (2003) Surf Rev Lett 10:233–239
55. Banhart F, Ajayan PM (1996) Nature 382:433–435
56. Banhart F (1997) J Appl Phys 81:3440–3445
57. Davison BN, Picket W (1994) Phys Rev B 49:14770

http://www.springer.com/978-1-4419-0530-7

Nanodiamonds
Applications in Biology and Nanoscale Medicine
Ho, D. (Ed.)
2010, XV, 286 p., Hardcover
ISBN: 978-1-4419-0530-7